Methanol Synthesis Over PdIn, In2O3, and CuZn From First-Principles Microkinetics: Similarities and Differences

Citation for the original published paper (version of record):
Kauppinen, M., Posada Borbon, A., Grönbeck, H. (2022). Methanol Synthesis Over PdIn, In2O3, and CuZn From First-Principles Microkinetics: Similarities and Differences. Journal of Physical Chemistry C, 126(36): 15235-15246.
http://dx.doi.org/10.1021/acs.jpcc.2c05715

THE JOURNAL OF PHYSICAL CHEMISTRY C
A JOURNAL OF THE AMERICAN CHEMICAL SOCIETY

pubs.acs.org/JPCC

Article

Methanol Synthesis Over PdIn, In_2O_3, and CuZn From First-Principles Microkinetics: Similarities and Differences

Minttu Kauppinen,* Alvaro Posada-Borbón, and Henrik Grönbeck*

Cite This: *J. Phys. Chem. C* 2022, 126, 15235−15246

Read Online

ACCESS | Metrics & More | Article Recommendations | Supporting Information

ABSTRACT: Methanol synthesis via catalytic CO_2 hydrogenation is an important reaction where a valuable fuel and chemical is produced from a greenhouse gas. In_2O_3- and Pd-promoted In_2O_3 have experimentally shown promising activity and selectivity, although the nature of the active sites remains under debate. In this study, the kinetic behavior of potential active sites in Pd-promoted In_2O_3 toward methanol synthesis and the competing reverse water−gas shift reaction is assessed by exploring pristine In_2O_3 and a PdIn intermetallic phase by using first-principles mean-field microkinetics. The PdIn intermetallic phase is modeled with PdIn(310) and In_2O_3 with In_2O_3(110). The results are compared to Zn-decorated Cu(211), representing the commercial Cu/ZnO-based catalyst. PdIn shows better performance than both the unpromoted In_2O_3 and Zn-decorated Cu at conditions relevant to the industrial process. For all three systems we find that stabilization of adsorbed hydrogen enhances activity toward methanol, which provides insights for further catalyst development.

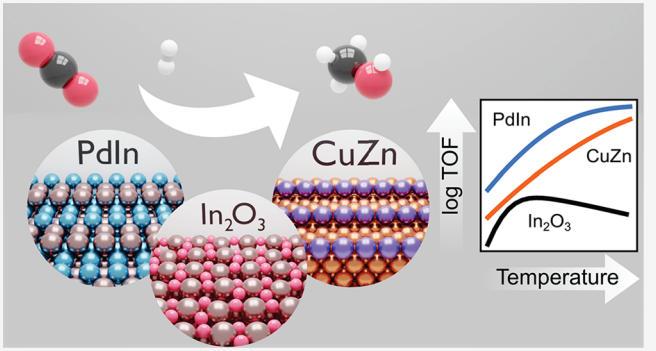

1. INTRODUCTION

Direct methanol synthesis using carbon dioxide as a feedstock is an important process, which utilizes CO_2 for production of a valuable platform and fuel molecule.[1−3] However, the commercial $Cu/ZnO/Al_2O_3$ catalysts are optimized for a mixed feed of CO and CO_2[4] and suffer from low selectivity and stability with a CO_2-only feed due to the competing reverse water−gas shift (RWGS) reaction and water formation.[4−6] Recent focus has therefore been to explore novel materials that can selectively convert CO_2 to methanol while maintaining high stability.[1]

Indium oxide-based materials have been put forward as promising candidates for methanol synthesis catalysts, and they have been shown to outperform the commercial Cu-based catalysts in terms of selectivity and stability.[7−10] Moreover, the performance of In_2O_3-based catalysts can be further enhanced by promotion with palladium.[8−12] Different alternative active sites have been proposed to explain the observed promotion: (1) Formation of an active PdIn intermetallic phase,[9,11] (2) active Pd nanoparticles on In_2O_3,[12] (3) highly dispersed Pd single atoms on In_2O_3,[10,13] (4) synergestic activity between In_2O_3 and PdIn,[9] and (5) formation of a reactive Pd/In_2O_3 interface.[12] The Pd derived sites in the Pd/In_2O_3 materials are usually suggested to promote the reaction by lowering the barrier for hydrogen activation,[10,12] although Pd-only catalysts show poor activity[11] and selectivity[9,10] toward methanol despite nonactivated H_2 dissociation. It should be noted that Pd and In_2O_3 interact strongly, and the intermetallic PdIn phase is readily obtained in the presence of hydrogen by a reactive metal−support interaction (RMSI) at moderate temperatures.[14−16]

Methanol synthesis has previously been studied over the PdIn (110), (211), and (310) surfaces using Density Functional Theory (DFT) calculations and mean-field microkinetic (MFMK) modeling.[17,18] The PdIn(310) surface was identified as a possible active phase. The preferred pathway from CO_2 to methanol was found to be the formate route, with HCOOH hydrogenation to H_2COOH being the rate-determining step. However, desorption of CO into the gas phase was not included in these studies, which excludes the evaluation of selectivity toward methanol synthesis with respect to the RWGS reaction. The behavior of the unpromoted In_2O_3 material toward methanol synthesis and RWGS was recently studied using a first-principles based microkinetic model,.[19] The reaction was also in this case found to proceed through the formate route, and the main rate controlling step was found to be the dissociation of the H_2COOH intermediate into H_2CO (formaldehyde) and an OH group. Several DFT and microkinetic studies have been conducted for the commercial $Cu/ZnO/Al_2O_3$ catalyst using

Received: August 10, 2022
Revised: August 17, 2022
Published: September 2, 2022

https://doi.org/10.1021/acs.jpcc.2c05715
J. Phys. Chem. C 2022, 126, 15235−15246

the Cu(211) and Zn decorated Cu(211) to model the active sites.[20−22] On the CuZn model sites, the reaction can occur via the formate route from CO_2 or the formyl route from CO. The rate controlling steps for the formate and formyl pathways have been found to be HCOOH hydrogenation and HCO hydrogenation, respectively.[23,24] Although the involvement of other active sites such as metal-oxide interfaces[25,26] also could contribute to the activity of the catalyst, the alloy models have been used to achieve good agreement between kinetic models and experiments.[23] It is clear that the $Cu/ZnO/Al_2O_3$ system serves as a good point of comparison to assess the performance of the PdIn(310) and In_2O_3 models.

The performance of PdIn nanoparticles, unpromoted In_2O_3, and commercial $Cu/ZnO/Al_2O_3$ samples have been compared experimentally for liquid phase methanol synthesis.[11] The Pd promoted In_2O_3 nanoparticles showed considerably higher activity (70% higher) and superior methanol selectivity (over 90%) compared to the commercial catalyst at 210 °C. In_2O_3 showed modest activity, whereas metallic Pd particles did not show any activity for neither methanol synthesis nor RWGS. For gas-phase methanol synthesis, the PdIn intermetallic catalyst supported on SiO_2 have been measured to outperform the unpromoted In_2O_3 supported on SiO_2, reaching activities 3 to 6 times higher than that of In_2O_3 and higher selectivities of 23−61% (compared to 24%).[9] However, it is often difficult to compare the intrinsic activities of multicomponent catalyst samples experimentally due to uncertainties with respect to the number of active sites. A comprehensive comparison of experimental activity and selectivity over promoted In_2O_3 and Cu-based catalysts was presented in ref 27. To the best of our knowledge, no direct comparison has been previously attempted between the PdIn alloy, unpromoted In_2O_3 and the commercial catalyst using computational methods. From the diverging reports, it is clear that a more fundamental understanding of the reaction mechanism over the possible active sites present in these materials is required.

In this study, we employ density functional theory calculations and mean-field microkinetic simulations to analyze the reaction mechanism, activity, and selectivity of the methanol synthesis reaction over the PdIn intermetallic compound. Furthermore, we directly compare the performance of the PdIn(310) model system to that of $In_2O_3(110)$ and CuZn(211), which serve as models for the unpromoted oxide and the commercial $Cu/ZnO/Al_2O_3$ catalyst, respectively. Our results show that the PdIn(310) surface has the highest methanol activity in the 200−240 °C temperature regime followed by CuZn and In_2O_3. The RWGS reaction is not active on the PdIn and CuZn systems at the studied temperatures, indicating that a different site could be responsible for the unwanted side reaction experimentally. On the PdIn system, the inactivity toward RWGS is due to the strong adsorption of CO to the Pd sites. In contrast to the two alloys, a switch-over from methanol to CO selectivity is observed over In_2O_3. Methanol is over all systems mainly produced from CO_2 via the formate pathway. In addition, CO hydrogenation contributes to methanol formation via the formyl pathway on CuZn and on the Pd site on PdIn. On all systems, the most abundant surface intermediate is formate, which inhibits the reaction rate by site blocking. Increasing the hydrogen adsorption strength is found to enhance the reaction rate on all systems regardless of the overall reaction mechanism and the rate-determining step. However, the activation energy for H_2 dissociation has no appreciable kinetic control, even in cases where the barrier is high. The kinetic dependence on hydrogen adsorption energy is likely common to many other systems that catalyze the CO_2/CO hydrogenation to methanol, and we propose that the activity in many cases could be enhanced by the presence of sites that stabilize hydrogen adsorption.

2. COMPUTATIONAL METHODS

The electronic structure calculations were performed using the Vienna Ab initio Simulation Package (VASP; version 5.4.4).[28−31] The BEEF-vdW functional was used, as dispersion forces have been previously found to have a significant effect on the energetics of the methanol synthesis reaction on metal surfaces.[20] The metal bulk structures were optimized using a 800 eV plane-wave cutoff and a 16 × 16 × 16 Monkorst-Pack mesh. The optimized lattice constant for the PdIn, which adopts the CsCl structure, is 3.34 Å, and the Cu fcc lattice constant is 3.66 Å. Both values are in fair agreement with the experimentally determined parameters of 3.24 Å[32] and 3.62 Å[33] for PdIn and Cu, respectively. Vibrational analysis was performed by finite differences. Transition states were obtained using climbing-image nudged elastic band (CI-NEB) method,[34] and verified by the presence of a single imaginary mode along the reaction coordinate.

The PdIn(310) surface was modeled with a p(4 × 4) surface slab of 13.23 × 10.50 Å lateral dimensions with five atomic layers. The three top layers were allowed to relax whereas the two bottom layers were fixed to the bulk positions. The (310) surface has two step-edges; one with a row of Pd atoms, and one with a row of In atoms (see Figure 1a). The (310) surface has a similar active site as the fcc metal (211) surface as the edge combines microfacets with 4-fold and 3-fold hollow sites.[18]

The commercial Cu-based catalyst was modeled either with Cu(211) or a Zn-decorated Cu(211), see Figure 1b. The two models were treated with (3 × 1) surface cells of lateral dimensions 6.34 × 10.40 Å with five atomic layers, with the three bottom layers fixed at the Cu bulk positions. Cu(211) and Zn substituted Cu(211) slabs have been used in previous studies[20−22] as the pure Cu edge and the fully Zn substituted edge represent the limiting cases for the atomic composition of the substitutional CuZn alloy. The slabs were separated by at least 12 Å vacuum in the direction perpendicular to the surface. The active site of the unpromoted In_2O_3 was modeled with a (1 × 1) $In_2O_3(110)$ surface cell with lateral dimensions 14.60 × 10.30 Å, see Figure 1c. The DFT results for the $In_2O_3(110)$ model were taken from our previous study.[19] It has previously been suggested that oxygen vacancies affect the methanol synthesis reactions from CO_2 over In_2O_3.[7] The presence of vacancies have been inferred from X-ray photoelectron spectroscopy (XPS) measurements showing a positive shift in the O 1s binding energy compared to binding energy of oxygen in the bulk oxide. However, we have recently shown that oxygen vacancies do not result in positive shifts in the O 1s binding energy.[35,36] Instead, we suggest that the higher O 1s binding energies originates from a hydroxylated surface. Oxygen vacancies are probably present experimentally, however, the correlation between the amount of vacancies and the In_2O_3 activity appears to be unclear at this point. It could be noted that surface hydroxylation as well as the presence of oxygen vacancies change the oxidation state of In.

As the DFT data is used in a microkinetic model, it is important that the overall gas-phase thermodynamics is

https://doi.org/10.1021/acs.jpcc.2c05715
J. Phys. Chem. C 2022, 126, 15235−15246

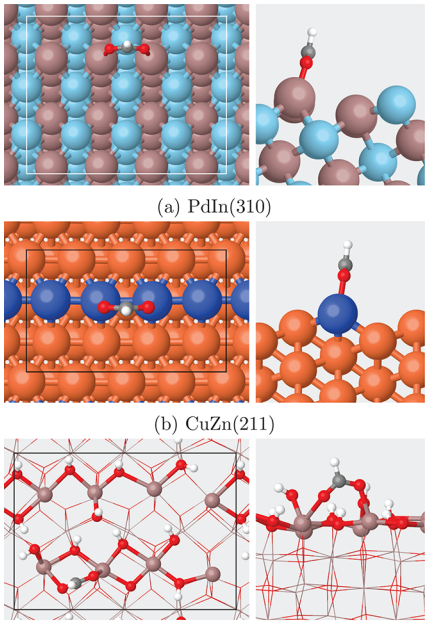

Figure 1. Structural models with adsorbed formate in top (left) and side (right) views of a) PdIn(310), b) CuZn(211) and c) hydroxylated In_2O_3(110). The In, Pd, Zn, Cu, O, C and H atoms are colored beige, light blue, blue, orange, red, gray, and white, respectively. For clarity, the adsorbate atoms and topmost In and O atoms are shown with balls and sticks, while the rest are shown with lines. The surface cells are indicated with white/black rectangles in the top-view.

properly described. In particular, it is important that the enthalpy changes in the methanol synthesis and RWGS reactions are close to the experimental values.[20] To obtain reasonable enthalpy changes for the overall reactions, a correction to the DFT values was introduced for the gas-phase species. The corrections were evaluated by minimizing the mean absolute errors between the experimental and DFT calculated reaction energies for a set of gas-phase reactions, see Supporting Information (SI). A similar approach has been employed in previous DFT-based microkinetic studies of methanol synthesis from CO_2.[19−21] The explored reaction network consists of 15 reactions (see Table 1). Reactions R1−R10 are the formate pathway for CO_2 to methanol, R11−R13 are the RWGS reaction, and R14 and R15 are steps included to form methanol from CO via the formyl route.

The potential energy surfaces connected to the 15 reactions were evaluated for the different catalyst models. Two separate dual site microkinetic models were constructed to describe the reaction over PdIn and CuZn, respectively. Diffusion between Pd and In sites or Cu and Zn sites was not considered in the final model. The reactants were not allowed to react "across sites", for example, a reaction between a formate on an In site and a hydrogen on a Pd site was not allowed. This is a reasonable approximation given the large distance (ca. 5 Å) between the edges. For the PdIn system, the microkinetic model was constructed with 27 reactions. As CO does not adsorb on the In site, reactions R13, R14, and R15 were not included for the In site. Thus, R12 was modified for the In site so that CO desorbs to the gas-phase after the reaction. For the CuZn system, the microkinetic model consisted of a total of 30 reactions, as all 15 reactions can take place on either the pure Cu or the Zn-decorated step-edge.

Table 1. List of Elementary Reactions Occurring on Active Site * (= Pd, In, Cu, Zn); Occupation of Two Sites is Indicated by **

reaction	
$H_2(g) + 2^* \rightleftharpoons 2H^*$	(R1)
$CO_2(g) + H^* + * \rightleftharpoons HCOO^{**}$	(R2)
$HCOO^{**} + H^* \rightleftharpoons HCOOH^{**} + *$	(R3)
$HCOOH^{**} + H^* \rightleftharpoons H_2COOH^{**} + *$	(R4)
$H_2COOH^{**} \rightleftharpoons H_2CO^* + OH^*$	(R5)
$OH^* + H^* \rightleftharpoons H_2O^* + *$	(R6)
$H_2O^* \rightleftharpoons H_2O(g) + *$	(R7)
$H_2CO^* + H^* \rightleftharpoons H_3CO^* + *$	(R8)
$H_3CO^* + H^* \rightleftharpoons CH_3OH^* + *$	(R9)
$CH_3OH^* \rightleftharpoons CH_3OH(g) + *$	(R10)
$CO_2(g) + H^* + * \rightleftharpoons COOH^{**}$	(R11)
$COOH^{**} \rightleftharpoons CO^* + OH^*$	(R12)
$CO^* \rightleftharpoons CO(g) + *$	(R13)
$CO^* + H^* \rightleftharpoons HCO^* + *$	(R14)
$HCO^* + H^* \rightleftharpoons H_2CO^* + *$	(R15)

Each individual site in the model has a site balance according to

$$\sum_i n\theta_i = 1 - \theta_* \tag{1}$$

where θ_i is the fractional coverage of surface species i, θ_* is the coverage of the empty site (In, Pd, Zn, Cu), and n is the number of sites that species i occupies on the surface ($n = 1$ for small species such as H, and $n = 2$ for bulky bidentate species like HCOO, see Table 1).

The rate constants for activated surface reactions were calculated according to transition state theory:

$$k = \frac{k_B T}{h} \exp\left[\frac{\Delta S^{\ddagger}}{k_B}\right] \exp\left[-\frac{\Delta E^{\ddagger}}{k_B T}\right] \tag{2}$$

where k_B is the Boltzmann constant, T is the temperature, h is Planck's constant, $\Delta E^{\ddagger}$ is the energy between the initial state and the transition state, including the zero point energy correction, and $\Delta S^{\ddagger}$ is the corresponding change in entropy. For surface species, the entropy was evaluated in the harmonic approximation, whereas the gas-phase species were treated with the ideal-gas approximation.

The forward rate constants for adsorption were calculated according to the collision theory:

$$k_{ads} = s(\theta)\frac{pA_{ads}}{\sqrt{2\pi m k_B T}} \tag{3}$$

where A_{ads} is the area of the site (area of the surface slab divided by the number of surface layer atoms), p is the partial pressure of the gas, and m is the mass of the gas molecule. The sticking coefficient $s(\theta)$ was in all cases set to unity. To ensure that the model remains thermodynamically consistent, the reverse rate constant for each elementary step was calculated

https://doi.org/10.1021/acs.jpcc.2c05715
J. Phys. Chem. C 2022, 126, 15235−15246

by dividing the forward rate constant with the equilibrium constant.

The mean-field microkinetic model was solved numerically using a Python based code. The numerical integration was performed using the solve_ivp function implemented in the Scipy package[37] scipy.integrate. The microkinetic results for the $In_2O_3(110)$ surface were taken from ref 19.

The simulations were performed at differential conditions of 30 bar of H_2, 10 bar of CO_2, and 1 bar of each of H_2O, CO, and methanol. The gas-phase compositions correspond to typical experimental conditions during methanol synthesis at low CO_2 conversion. The integration was performed for long time intervals (typically 10^6 s) to ensure that a steady-state was reached. Furthermore, the changes in surface concentration were checked against a criterion that the rate of change in surface concentration $\frac{d\theta_i}{dt}$ was below 0.00001 s^{-1} at the end of the simulation.

The microkinetic results were analyzed by calculating the degree of rate control (DRC)[38] of each elementary step i toward the total rate r:

$$\mathrm{DRC}_i = \frac{k_i}{r}\left(\frac{\partial r}{\partial k_i}\right)_{k_{j\neq i},K_i} \tag{4}$$

where r is the rate of the net reaction and k_i is the rate constant of elementary step i. The rate constants of all other reactions and all equilibrium constants were kept unchanged while the derivative was taken against k_i. The rate constants were changed by 1% from their initial values. The DRC sum rule[38] is upheld at all temperatures, that is, the DRC of all steps sum to ≈1.00. The reaction kinetics were also analyzed with respect to the reaction orders. Reaction order n_i of a gas-phase species i with respect to the net rate r is defined as

$$n_i = \frac{\partial \ln r}{\partial \ln p_i} \tag{5}$$

where p_i is the partial pressure of the gas. The reaction orders were calculated with respect to the rate of methanol production.

3. RESULTS

The reaction network for the methanol synthesis process comprises three net reactions with experimental reaction enthalpies:[39]

$$3H_2 + CO_2 \rightleftharpoons CH_3OH + H_2O \quad \Delta H^\circ = -53 \text{ kJ mol}^{-1}$$

$$2H_2 + CO \rightleftharpoons CH_3OH \quad \Delta H^\circ = -95 \text{ kJ mol}^{-1}$$

$$H_2O + CO_2 \rightleftharpoons H_2 + CO \quad \Delta H^\circ = +40 \text{ kJ mol}^{-1}$$

The first two reactions are methanol synthesis from CO_2 and CO, whereas the third reaction is the competing RWGS. The reaction network for the three net reactions is presented graphically in Figure 2. CO_2 hydrogenation to methanol follows the formate (HCOO) pathway, whereas CO hydrogenation to methanol proceeds via the formyl (HCO) pathway. The explored reaction pathways are based on suggestions in the literature and should capture the main routes although additional pathways and side reactions are possible.

Both formate and formyl pathways start with the dissociative adsorption of hydrogen. In the next step, CO_2 or CO adsorbs on the surface and reacts with the adsorbed hydrogen forming HCOO (formate) or HCO (formyl), respectively. The rest of the pathways comprise several hydrogenation steps. The formate species is hydrogenated twice forming a H_2COOH species, which dissociates into H_2CO (formaldehyde) and an OH group. The OH group reacts with hydrogen to form water, which desorbs. In the formyl pathway, the formyl species is converted directly into H_2CO by reacting with hydrogen. The two pathways coincide after the formation of H_2CO, and methanol is produced from H_2CO via subsequent hydrogenation of its carbon and oxygen atoms. The third net reaction in the cycle is the unwanted RWGS reaction, which lowers the selectivity toward methanol. The RWGS pathway starts with the reaction between surface hydrogen and CO_2, forming a COOH (carboxyl) intermediate instead of HCOO. The COOH intermediate dissociates into OH and CO, with OH reacting with H to produce water, whereas CO desorbs.

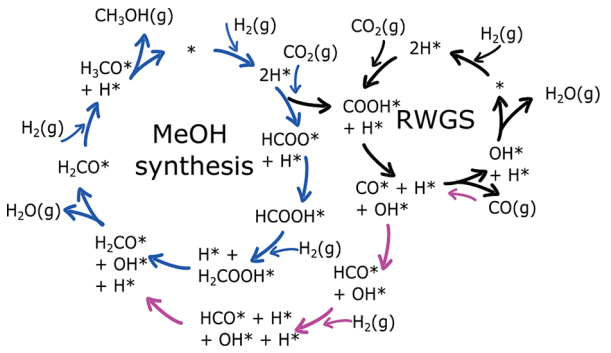

Figure 2. Catalytic cycle for methanol synthesis from CO_2 and CO showing the formate pathway (blue), formyl pathway (pink), and the reverse water−gas shift reaction (black).

Potential Energy Landscapes. The calculated energy landscapes for methanol synthesis ($3H_2 + CO_2 \rightarrow CH_3OH + H_2O$) on PdIn(310) and Cu(211)/CuZn(211) are shown in Figures 3 and 4 together with structural models of selected intermediates.

Hydrogen Dissociation. The first step in the reaction is H_2 adsorption. The barrier for H_2 dissociation on PdIn(310) is very different on the Pd and In sites. Hydrogen dissociation on the Pd site has a barrier of 0.45 eV, and the adsorption energy is −0.14 eV. The barrier on the In site is 1.01 eV and the reaction is endothermic by 0.47 eV. On the Cu and Zn step-edge, the dissociation barriers are 0.71 and 1.27 eV, respectively, whereas adsorption energies are −0.06 and 0.29 eV, respectively. Compared to the hydrated $In_2O_3(110)$ surface from our previous study (E_{act} = 0.84 eV, E_{ads} = −0.02 eV),[19] dissociative adsorption of hydrogen proceeds with a lower barrier and is more exothermic on the Pd and Cu sites, whereas it is less facile on the In and Zn sites.

Formate Pathway. The next step in the potential energy landscape is CO_2 adsorption. CO_2 adsorbs by reacting directly with hydrogen forming formate. On all four investigated surface sites, as well as on $In_2O_3(110)$, formate adsorbs in a bidentate configuration atop two metal atoms. The barrier for the reaction is low on the Pd and In edge (0.38/0.47 eV on Pd/In), which indicates that formate should form easily on the surface. The reaction energy is ΔE = −0.52 eV on the Pd edge, and ΔE = −1.05 eV on the In edge, although the stability of formate with respect to the gas-phase is similar. The formate formation barrier is low also on the Cu and Zn edge sites (0.29/0.40 eV for Cu/Zn), and is strongly exothermic (−1.11/

https://doi.org/10.1021/acs.jpcc.2c05715
J. Phys. Chem. C 2022, 126, 15235−15246

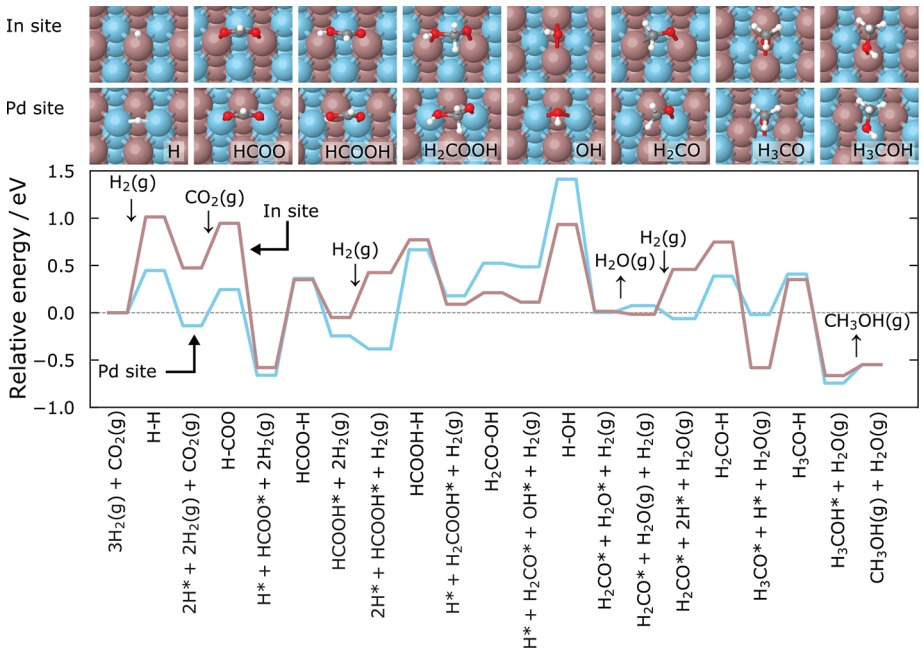

Figure 3. Zero-point corrected energy landscape of the $CO_2 + 3H_2 \rightarrow CH_3OH + H_2O$ reaction on PdIn(310). All energies are with respect to the clean surface and CO_2 and $3H_2$ in the gas phase. The atoms in the structure images are colored using the same scheme as in Figure 1a.

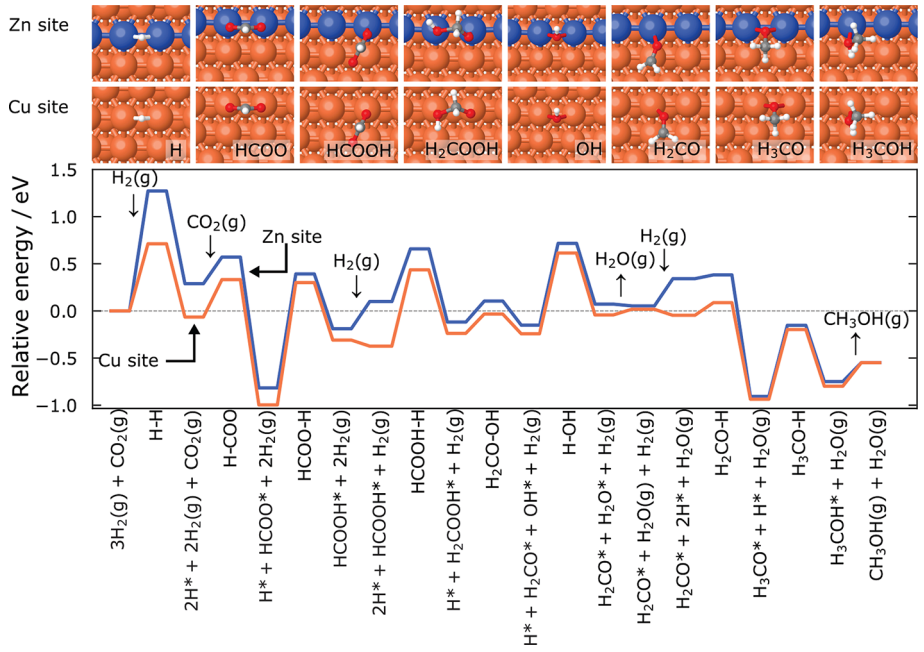

Figure 4. Zero-point corrected energy landscape of the $CO_2 + 3H_2 \rightarrow CH_3OH + H_2O$ reaction on Cu(211)/CuZn(211). All energies are with respect to the clean surface and CO_2 and $3H_2$ in the gas phase. The atoms in the structure images are colored using the same scheme as in Figure 1a.

−0.93 eV for Cu/Zn). Compared to the alloy sites, formate formation is even more favored on the In_2O_3, as the barrier is only 0.17 eV and the reaction is highly exothermic (ΔE = −1.17 eV).

The hydrogenation of formate into HCOOH (formic acid) has a large barrier of 1.02 and 0.93 eV on the Pd and In edge sites, respectively, and is endothermic (ΔE = 0.42 and 0.53 eV, respectively). The subsequent hydrogenation of formic acid into H_2COOH is less favorable on the Pd site compared to the In site as the barrier is substantially higher (1.04 vs 0.35 eV) and is thermodynamically disfavored (ΔE = 0.56 vs −0.33 eV).

Formate hydrogenation is energetically costly also on CuZn(211), with a barrier of 1.30/1.21 eV and a reaction energy of 0.69/0.63 eV on the Cu/Zn edge site. The next hydrogenation step is more favorable on the Zn site compared to the Cu site; the barrier is 0.56 compared to 0.81 eV and the reaction energy is −0.22 compared to 0.14 eV. On In_2O_3, hydrogenation of formate has a large barrier (0.72 eV) and is endothermic by 0.65 eV. The subsequent hydrogenation of formic acid to H_2COOH on In_2O_3 has a barrier and reaction energy of 0.24 and −0.32 eV, which is similar to the In edge of the PdIn(310) system.

https://doi.org/10.1021/acs.jpcc.2c05715
J. Phys. Chem. C 2022, 126, 15235−15246

All reactions on PdIn and CuZn occur at the edge and the dissociation of H_2COOH proceeds by detaching OH from the H_2CO fragment. The barrier is 0.34 eV on the Pd edge and the reaction is endothermic by 0.31 eV. The barrier is low (0.12 eV) on the In edge, and the reaction is thermoneutral. The OH group prefers to adsorb in a bridging position on both edges, however, in different configurations. OH adsorbs perpendicular to the In step-edge, whereas OH is parallel to the Pd step-edge. The reaction energetics are similar on the two metal edges on CuZn and the In edge of PdIn. The barriers are low (0.20 and 0.22 eV on Cu and Zn, respectively) and the reaction is thermoneutral. The OH group binds in the parallel bridging position on both Cu and Zn step-edges.

The last two steps in the formate pathway are the two hydrogenation steps of the H_2CO species to form methanol. The energetics for the Pd edge are different compared to the three other alloy sites. For Pd, the hydrogenation of the carbon atom on H_2CO is thermoneutral, and the subsequent hydrogenation of the oxygen atom is strongly exothermic. The situation is reversed on the In, Cu, and Zn sites, where the first hydrogenation step is strongly exothermic with a low barrier, whereas the last hydrogenation reaction has a larger barrier and is close to thermoneutral. On In_2O_3, the dissociation step was found to be associated with a barrier of 0.90 eV, which is the highest along the reaction pathway.

Formyl Pathway. The direct reaction between CO and adsorbed hydrogen is the first step in the formyl pathway. The reaction is not feasible on the In edge, as CO does not adsorb to the In site. CO binds strongly on the Pd site, and formyl formation has a barrier of 1.05 eV and is endothermic by 0.76 eV. As the barrier for formyl formation is the same as the highest barrier in the formate route on the Pd site, the formyl pathway could contribute to the overall mechanism. The formyl route may contribute on CuZn(211) as well, as the highest barrier (formyl formation) in the formyl pathway on CuZn(211) is 0.96 and 0.38 eV on the Cu and Zn sites, respectively.

Reverse Water–Gas Shift Reaction. A competing reaction for CO_2 hydrogenation to methanol is the reverse water–gas shift reaction, where CO_2 is first hydrogenated at the oxygen forming a COOH intermediate instead of formate. The formation of the COOH (carboxyl) intermediate from adsorbed hydrogen and CO_2 has a barrier of 1.15 and 1.10 eV at the Pd and In edge sites, respectively. The reaction is slightly endothermic (0.23 eV) on the Pd site, and thermoneutral on the In site. Carboxyl formation has high barriers of 1.30 and 1.32 eV on the Cu and Zn edge sites, respectively, and is thermoneutral. As carboxyl formation is associated with a much higher barrier and is less stable than formate on all four alloy sites, as well as on $In_2O_3(110)$,[19] formate formation is expected to dominate over carboxyl formation at low temperatures. However, the dissociation of carboxyl has a low barrier of 0.25 eV on the Pd edge site, and is exothermic by −0.51 eV. Therefore, RWGS may compete with methanol synthesis at the Pd edge, as the highest barriers in the RGWS, formate, and formyl pathways are comparable, 1.15 eV (carboxyl formation), 1.04 eV (HCOOH hydrogenation), and 1.05 eV (formyl formation).

Microkinetic Analysis. *Rates, Coverages, and Apparent Activation Energies.* The microkinetic analysis was performed at 30:10:1:1:1 bar of $H_2/CO_2/CH_3OH/H_2O/CO$ and reveals how the activity toward methanol synthesis and the RWGS differ between the three surfaces, see Figure 5. On PdIn, the

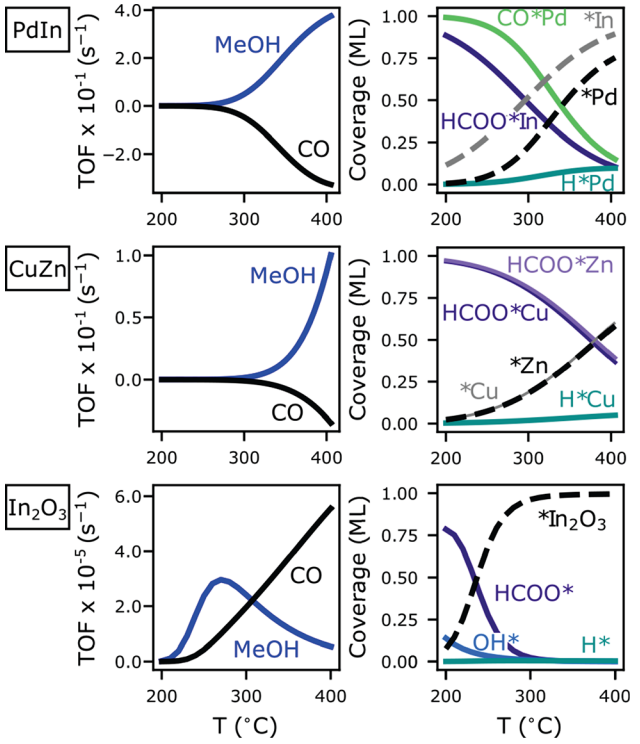

Figure 5. Left: Methanol and CO turnover frequencies (TOF) as a function of temperature for PdIn (top), CuZn (middle), and In_2O_3 (bottom). Right: Corresponding coverages. Only surface species with coverage above 0.01 ML are shown. Note that the coverage of HCOO at each site is scaled up by a factor of 2. The microkinetic simulations were performed at 30:10:1:1:1 bar of $H_2/CO_2/CH_3OH/H_2O/CO$. Note that the methanol originates from both CO_2 and CO hydrogenation.

methanol production starts slightly below 300 °C, and continues to increase over the studied temperature range. The rate for methanol production is higher on Pd than In. However, all methanol produced on the Pd site originates from CO through the formyl pathway, whereas CO_2 is the preferred reagent on the In site. Approximately 10% of methanol is formed through the CO_2 hydrogenation pathway on In. CO is consumed in the reaction. Thus, the TOF of CO production remains negative in the shown temperature range, which means that the methanol selectivity is 100%.

For PdIn, the In site has a high formate coverage at low temperatures, and the onset of the methanol production from the In site coincides with the formate coverage falling below half a monolayer. The Pd site is completely blocked by CO at 200 °C, however, the CO coverage decreases with temperature, enabling methanol production once the CO coverage is below 0.75 ML. A low coverage of hydrogen is observed at temperatures where CO does not poison the Pd site. At temperatures higher than presented in Figure 5, a switch-over in selectivity toward RWGS is observed at about 600 °C. At this temperature, the selectivity toward methanol is 96% on the In site, whereas the selectivity toward CO is 73% on the Pd site, that is, Pd is the active site for RWGS.

The rate of methanol production on CuZn starts at a higher temperature than on PdIn, and the maximum TOF is approximately a 0.25% of that of PdIn at 400 °C. The TOF of CO production is also negative on the CuZn system, that is, CO is consumed to produce methanol. At the Cu site, the rate of the CO to methanol pathway is higher than the rate of the

https://doi.org/10.1021/acs.jpcc.2c05715
J. Phys. Chem. C 2022, 126, 15235−15246

CO_2 to methanol pathway below 360 °C, after which the CO_2 to methanol rate dominates. At the Zn site, the CO_2 to methanol pathway dominates at all temperatures. The difference between Cu and Zn sites in the preference for CO versus CO_2 as the reactant has been previously reported for similar microkinetic models over the Cu(211) and CuZn(211) surfaces.[21] Both Cu and Zn sites are completely covered by formate at low temperatures, and the formate coverage decreases at a higher temperature compared to the PdIn case. The high formate coverage is related to a stronger adsorption energy and a higher barrier for formate hydrogenation. On the Cu site, the only additional surface species with a non-negligible coverage is hydrogen.

In contrast to the two alloy systems, the methanol synthesis reaction over In_2O_3 starts at a much lower temperature of about 200 °C and goes through a maximum at approximately 270 °C. The switch-over in selectivity toward RWGS occurs at about 300 °C, which is a lower temperature than for PdIn and CuZn. As for the metals, In_2O_3 is occupied mainly by formate at low temperatures, and the onset of the methanol synthesis coincides with a lowering of the formate coverage, similarly to the metallic systems.

The TOF of methanol production at 240 °C, a temperature relevant to the industrial process, increases in the order In_2O_3 < CuZn < PdIn. The PdIn system clearly outperforms the other two systems in terms of activity toward methanol synthesis, with the TOF on PdIn being 30 times higher than on CuZn and 95 times higher than on In_2O_3. The computed selectivity toward methanol is at 240 °C 88% on the In_2O_3, whereas it is 100% on the PdIn site. However, methanol is produced both through CO hydrogenation and CO_2 hydrogenation on the PdIn and CuZn. Comparing the rate of only CO_2 hydrogenation, the TOF increases in the order CuZn < In_2O_3 < PdIn at 240 °C. The CO_2 hydrogenation rate is about 3 times higher over PdIn than over In_2O_3 and about 6 times higher than over CuZn.

Our calculated apparent activation energies for the PdIn, CuZn, and In_2O_3 systems are 157, 135, and 156 kJ mol^{-1}, respectively (see SI for Arrhenius plots). The apparent activation energies for PdIn and CuZn are larger than what has been previously experimentally determined for liquid phase methanol synthesis (35 and 41 kJ mol^{-1}, respectively[11]). It may seem surprising that the apparent activation energy for CuZn is lower than for PdIn, given that the TOFs are higher on PdIn. However, the apparent activation energies contain the effect of the coverages as well as the barriers of elementary surface reactions. The value for In_2O_3 is in good agreement with a previous computational and an experimental estimate,[10] although a lower value of about 92 kJ mol^{-1} have also been reported for experiments on In_2O_3.[13] Furthermore, it has been found that there is no correlation between the reaction rates and apparent activation energies for many In_2O_3 supported metal single-atom catalysts,[13] indicating that some other processes, such as transport phenomena, which do not have the same temperature dependence, also control the reaction rate.

Rate Control and Reaction Order Analysis. The kinetic bottlenecks in the potential energy surface can be obtained by doing a degree of rate control analysis. The results of the degree of rate control and reaction order analysis are shown in Figure 6. The three systems show large differences in their rate controlling steps. On the In site of the PdIn system, the methanol synthesis reaction proceeds through the formate pathway, and the sole rate controlling step at all temperatures is hydrogenation of HCOOH. At elevated temperatures, the formate formation reaction starts to have slight rate control (not shown). On the Pd site, the reaction follows the formyl pathway, and several hydrogenation steps have rate control, although hydrogenation of H_3CO to methanol has the highest rate control.

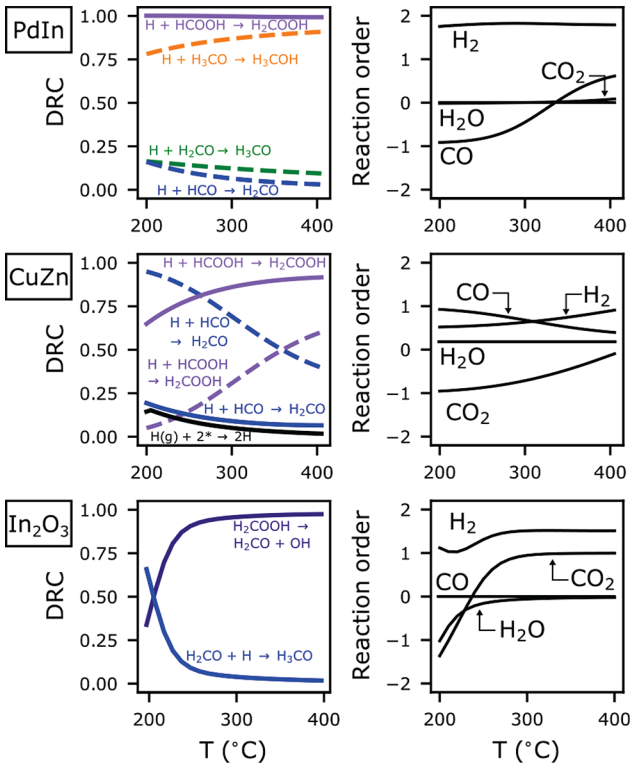

Figure 6. Degree of rate control (DRC) and reaction orders for the methanol synthesis reaction as a function of temperature for PdIn (top), CuZn (middle), and In_2O_3 (bottom). The DRC values for the PdIn and CuZn are presented separately at each site for the methanol production reaction. The Pd and Cu sites are shown with dashed curves and In and Zn sites with solid curves. The degree of rate control and reaction orders are shown only for steps/species with DRC/reaction order value larger than 0.05. The simulations were performed at 30:10:1:1:1 bar of $H_2/CO_2/CH_3OH/H_2O$:CO.

The situation on CuZn is more complex, which is expected because of the nested contributions from the formate and formyl pathways on both sites. On the Cu site, the hydrogenation of formyl to H_2CO controls the rate at low temperatures, whereas hydrogenation of HCOOH has a rate control at higher temperatures. The switch over in rate control is associated with the change in relative contributions from the formate and formyl pathways. On the Zn site, hydrogenation of HCOOH is dominating throughout the investigated temperature range. Hydrogen dissociation has some rate control on the Zn site, especially at low temperatures, which is related to the high dissociation barrier.

Over In_2O_3, the two rate controlling reactions are the hydrogenation of H_2CO, which dominates at temperatures below 200 °C, and the dissociation of the H_2COOH, which is the sole rate controlling step at temperatures above 250 °C.

The reaction kinetics could experimentally be characterized measuring reaction orders. Over PdIn, the reaction order of hydrogen is always positive and varies only slightly from 1.75 to 1.79 in the studied temperature range. The CO_2 reaction

https://doi.org/10.1021/acs.jpcc.2c05715
J. Phys. Chem. C 2022, 126, 15235−15246

order over PdIn is close to zero starting at −0.01 at low temperature, crossing over to positive values around 300 °C, and reaching a value of 0.08 at the highest temperature. The reason why the methanol production rate is insensitive to CO_2 is that the reaction rate is dominated by the formyl pathway at the Pd site. The reaction order of CO varies from −0.92 to 0.61. The negative reaction order at low temperature is explained by the high coverage of CO, and that increasing the CO pressure leads to site blocking. Over PdIn, we find that the reaction order with respect to H_2O and methanol are zero in the studied temperature range, which is a consequence of the low adsorption energies.

On CuZn, the reaction order in hydrogen varies between 0.52 and 0.93. The reaction order with respect to CO is positive, as it is a reactant in the formyl pathway and does not block any sites, unlike on PdIn. The reaction order of CO starts from 0.92 and gradually decreases with increasing temperature to reach a value of 0.34. The decrease in the reaction order is explained by the decreased importance of the formyl pathway when temperature is raised. The behavior of the CO_2 reaction order mirrors that of CO, varying from −0.95 to −0.07 with increasing temperature. The trend in the negative reaction order of CO_2 is due to the decreased site blocking by formate at higher temperatures.

The hydrogen reaction order over In_2O_3 has a minimum (with a positive value of ≈1) and increases at higher temperatures to a constant value of 1.5. The reaction orders of CO_2 and H_2O are both strongly negative at low temperatures. In similarity to CuZn, an increased CO_2 pressure leads to formate blocking of the surface at low temperatures. The CO_2 reaction order reaches a value of 1.0 as the temperature is increased. The negative reaction order of H_2O is due to site blocking by the created OH groups. This effect is reduced as water desorbs at high temperatures.

Simplified Rate Expression. Based on the results of steady-state coverages, degree of rate control, and reaction orders analyses, it is possible to formulate a simplified rate expression for methanol production over the surfaces. In the simplified form, the TOF is proportional to the product of the coverage of the most abundant surface species, coverage of empty sites, hydrogen pressure raised to (approximately) the power of the reaction order in hydrogen, and an exponential term containing the free energy of the transition state with the highest degree of rate control. The TOF at each active site in the studied models could in this way be expressed as

$$\mathrm{TOF}_{\mathrm{MeOH}}^{\mathrm{Pd}} = P_{\mathrm{H_2}}^{2}\theta_{\mathrm{CO}}\theta_{*}\frac{k_{\mathrm{B}}T}{h}\exp\left(\frac{-G_{\mathrm{H3CO\text{-}H}}}{k_{\mathrm{B}}T}\right) \quad (6)$$

$$\mathrm{TOF}_{\mathrm{MeOH}}^{In} = P_{\mathrm{H_2}}\theta_{\mathrm{HCOO}}\theta_{*}\frac{k_{\mathrm{B}}T}{h}\exp\left(\frac{-G_{\mathrm{HCOOH\text{-}H}}}{k_{\mathrm{B}}T}\right) \quad (7)$$

$$\mathrm{TOF}_{\mathrm{MeOH}}^{\mathrm{Cu}} = P_{\mathrm{H_2}}\theta_{\mathrm{HCOO}}\theta_{*}\frac{k_{\mathrm{B}}T}{h}\exp\left(\frac{-G_{\mathrm{HCOOH\text{-}H}}}{k_{\mathrm{B}}T}\right) \quad (8)$$

$$\mathrm{TOF}_{\mathrm{MeOH}}^{\mathrm{Zn}} = P_{\mathrm{H_2}}\theta_{\mathrm{HCOO}}\theta_{*}\frac{k_{\mathrm{B}}T}{h}\exp\left(\frac{-G_{\mathrm{HCOOH\text{-}H}}}{k_{\mathrm{B}}T}\right) \quad (9)$$

$$\mathrm{TOF}_{\mathrm{MeOH}}^{\mathrm{In_2O_3}} = P_{\mathrm{H_2}}^{1.5}\theta_{\mathrm{HCOO}}\theta_{*}\frac{k_{\mathrm{B}}T}{h}\exp\left(\frac{-G_{\mathrm{H_2CO\text{-}OH}}}{k_{\mathrm{B}}T}\right) \quad (10)$$

where P_{H_2} is the partial pressure of hydrogen, θ_i is the steady state coverage (obtained from the full microkinetic model) of a species i, whereas θ_* is the coverage of unoccupied sites. $G_{H3CO\text{-}H}$ is the free energy of the transition state of the methoxy hydrogenation reaction with respect to CO on the surface and two hydrogen molecules in the gas-phase, whereas $G_{HCOOH\text{-}H}$ is the free energy of the transition state of formic acid with respect to formate on the surface and one hydrogen molecule in the gas-phase. $G_{H_2CO\text{-}H}$ is the free energy of the H_2COOH dissociation transition state with respect to HCOO on the surface and one hydrogen molecule in the gas-phase. This analysis is similar to an energy span model,[40] including the effect of surface coverages. The simplified models are compared to the full microkinetic models in the SI. As reported in Figure 5, the coverage of CO and empty Pd sites on PdIn change faster with temperature than the coverage of HCOO and empty Cu on CuZn, resulting in a stronger temperature dependence, i.e. higher apparent activation energy. Meanwhile, the hydrogen pressure has a larger effect on the PdIn system (in line with the higher reaction order of hydrogen), resulting in a higher TOF. Another contributing factor to the higher observed TOF on PdIn is the free energy of the rate controlling transition state, which is slightly lower for PdIn than CuZn at low temperature. For the In_2O_3 system, the agreement between the TOF from the simplified rate expression and the full microkinetic model starts to deviate after the onset of the RWGS reaction, with the simplified expression being an overestimation of the full model result.

4. DISCUSSION

Having access to kinetic models for the three systems enables detailed comparisons of the kinetic behaviors and factors governing the reactions. Here we explore aspects of the kinetic model which could have a large effect on the behavior of the systems, namely the role of CO in the gas mixture, adsorbate stability, and coverage effects. Models for CO_2 hydrogenation have previously been constructed using reservoir sites,[18,21,23,41] that is, sites where H_2 can adsorb without competing with other adsorbates. Here we discuss the effect of hydrogen reservoir sites. The findings from the microkinetic models are also compared to previous experimental and computational studies.

Effect of Gas-Phase Composition. The presented microkinetic simulations were carried out at a gas-composition corresponding to about 10% yield for both methanol and CO. This enables methanol production from CO in addition to CO_2, mainly at the Cu and Pd sites. Additional microkinetic simulations were performed to explore the effect of removing CO from the gas-phase by setting the CO partial pressure close to zero (10^{-30} bar) while keeping the other pressures the same (30:10:1:1 bar of $H_2/CO_2/CH_3OH/H_2O$).

For PdIn, the simulations show that the Pd sites stay mainly unoccupied with a low coverage of hydrogen across the temperature range studied in the absence of CO in the gas-phase, and no methanol production from the Pd site is observed. In contrast to the case with CO in the gas-phase, production of CO is observed together with MeOH production. The selectivity to MeOH drops from virtually 100% across the studied temperature range to below 83% when only a trace of CO is allowed in the gas-phase. This indicates that at low conversions, the desorption of CO is favored over CO hydrogenation, which allows for the RWGS

https://doi.org/10.1021/acs.jpcc.2c05715
J. Phys. Chem. C 2022, 126, 15235−15246

reaction to compete. Additionally, in a CO_2 only feed, the In site is the main site for methanol synthesis. On the CuZn system, the absence of CO in the feed does not alter the selectivity toward MeOH or CO, however, the TOF for methanol synthesis is lowered because CO is the reactant in the formyl pathway. On CuZn, the RWGS reaction is limited by the high COOH formation barrier, and is therefore not enhanced by CO removal from the gas-phase. Unlike PdIn and CuZn, neither the activity nor selectivity toward methanol synthesis is affected by the presence of CO in the feed on In_2O_3, which is a consequence of the weak interaction between CO and In_2O_3.

Effect of Intermediate Stability. In our previous study, it was found that stabilizing certain intermediates, especially hydrogen, had a large enhancing effect on the methanol production rate.[19] Furthermore, the DRC analysis shows that the rate of reaction is highly dependent on hydrogenation reactions on all studied systems. The effect of intermediate stability on the methanol production TOF was here investigated by performing additional microkinetic simulations with modified equilibrium constants for some selected reactions. The analysis was performed for hydrogen adsorption, formate formation, formate hydrogenation, formic acid hydrogenation, CO hydrogenation, and formyl hydrogenation. The stability of the product species of the selected reactions were increased by 0.1 eV, and the response in the methanol production rate was calculated. The TOF as a function of temperature for the simulations with modified intermediate stabilities are presented in Figure 7. The modified

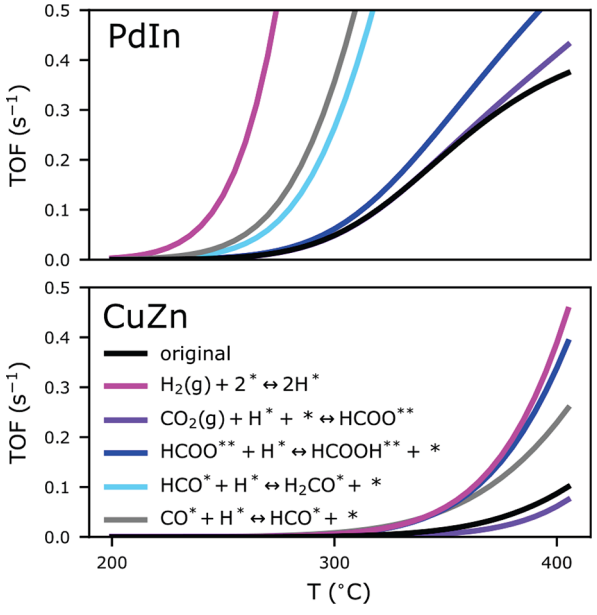

Figure 7. Effect of stabilizing selected intermediates on methanol synthesis TOF, calculated under the same conditions as the data in Figures 5 and 6. HCO* + H*↔ H_2CO^* + * did not change for CuZn and is not reported.

TOFs show that stabilizing hydrogen on the surface has the largest effect on the methanol synthesis activity on both PdIn and CuZn. The same result was obtained for the In_2O_3 system.[19] Besides hydrogen stabilization, the stabilization of formic acid (HCOOH) also leads to a significant increase in the methanol production rate. On the CuZn system, stabilization of formic acid leads to the preferred reagent switching from CO to CO_2. In a recent study, it was found that stabilization of formic acid could be achieved via hydrogen bonding to coadsorbed formate on the Cu(211) step edge, which resulted in an increased rate of methanol synthesis from CO_2.[42] The formate formation reaction has an appreciable effect on the TOF on all three model systems. On PdIn, the stabilization of the formate leads to a slightly increased TOF at high temperatures. Closer inspection shows that increasing the equilibrium constant of formate formation results in a lower TOF at low temperatures (not visible in Figure 7). On the CuZn system, the stabilization of formate always leads to a lower TOF, due to the general higher coverages of formate on CuZn. On both alloy systems, CO hydrogenation to formyl has a positive effect on the TOF as it enhances the rate for the formyl pathway. On PdIn, increasing the formyl hydrogenation equilibrium constant has a similar positive effect on the TOF. In summary, despite the large differences in the dominating mechanisms and activities over the three catalyst models, hydrogen stability is always a key factor for overall methanol synthesis activity, even in the absence of kinetic rate control by the hydrogen dissociation step. This is consistent with the fact that the reaction order is always positive with respect to the partial pressure of hydrogen.

Coverage Effects. The steady state coverages of formate (on In, Cu, and Zn sites) and CO (on Pd site) are high, especially at low temperatures. In the case of formate, the onset of methanol production is observed on all three surfaces at temperatures when formate coverage has dropped below 0.75 ML. The effect of the coverage on the potential energy landscape should therefore be investigated at high adsorbate coverages. In a previous first-principles study on the PdIn(310), formate coverage effects were included by calculating all intermediate energies and reaction barriers with a precoverage of 0.50 ML of formate on the surface, which resulted in a change in the preferred reaction mechanism from carboxyl pathway on clean PdIn(310) to the formate pathway.[18] Moreover, as already mentioned, the presence of formate enables a hydrogen bond assisted reaction path on Cu(211) which lowers the overall barrier to produce methanol from CO_2.[42] As shown in Figure 5, the CO coverage is high on the Pd site of PdIn. Generally, repulsive lateral interactions between neighboring CO molecules weaken the adsorption energy, which may lead to lower CO coverages. Interestingly, it has been found that the coverage of CO had little effect on the stability of other intermediates and transition states on Cu(211)[42] and PdIn(310).[18] Here, we investigate the effect of formate and CO coverage at the PdIn(310) edge sites.

We calculated the differential adsorption energies for formate on the In site and CO on the Pd edge site, as these are the most abundant surface species according to the microkinetic simulations (Top panel of Figure 8. The differential adsorption energy E_{diff} is defined as

$$E_{diff} = E_{slab+N} - E_{slab+(N-1)} - E_{ref}(g) \quad (11)$$

where E_{slab+N} is the total energy of the surface slab with N adsorbate molecules (with $N = 4$ defined as 1 ML), $E_{slab+(N-1)}$ is the total energy of the surface slab with $(N - 1)$ adsorbate molecules, and $E_{ref}(g)$ is the gas-phase reference energy. For formate, the reference is the total energy of CO_2 and half a hydrogen molecule in the gas phase, whereas for CO it is the total energy of a CO molecule in the gas phase. The second molecule of formate (0.50 ML) on the In site has a virtually identical differential adsorption energy to the first molecule.

https://doi.org/10.1021/acs.jpcc.2c05715
J. Phys. Chem. C 2022, 126, 15235−15246

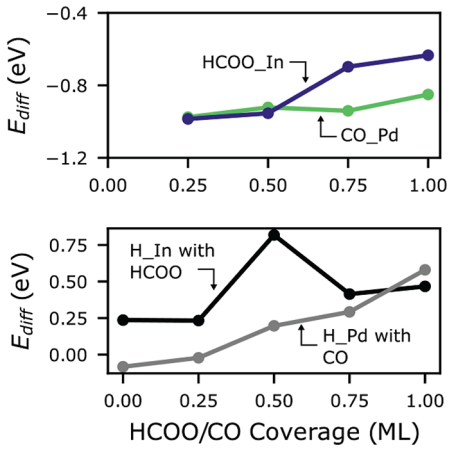

Figure 8. Top: Differential adsorption energies of formate on In step-edge, and CO on Pd step-edge as a function of coverage. Bottom: Differential adsorption energy of a hydrogen on the In step-edge site as a function of formate coverage and hydrogen on the Pd step-edge site as a function of CO coverage.

Note that due to their preferred bidentate adsorption configuration, two formate molecules occupy all four top sites on the In edge. In our microkinetic model, this is accounted for in the site balance, that is, formate formation requires one empty site in addition to the site occupied by the reacting hydrogen. To achieve a higher coverage of formate, some of the molecules have to adsorb perpendicular to the edge to free up a top site, which makes the adsorption less favorable. Strict mean-field approaches to reaction microkinetics do not account for local ordering of adsorbates. The adsorption energy of CO has a low coverage dependence on the Pd site, indicating that it is possible for CO to achieve a full monolayer coverage at the Pd edge. The results in Figure 8 are consistent with a previous study.[18]

As the stability of hydrogen has a major influence on the methanol production rate, it is important to consider how the coverage of formate and CO affect the adsorption energy of hydrogen. The differential adsorption energy of a hydrogen atom was evaluated with varying coverages of formate and CO at the In and Pd step-edge sites on PdIn(310) (Figure 8, bottom panel). The differential adsorption energy E_{diff} of hydrogen defined as

$$E_{diff} = E_{slab+H+N} - E_{slab+N} - \frac{1}{2}E_{H_2}(g) \quad (12)$$

where $E_{slab+H+N}$ is the total energy of the surface slab with one hydrogen atom and N adsorbate (HCOO or CO) molecules (with N = 4 defined as 1 ML), $E_{slab+(N)}$ is the total energy of the surface slab with N adsorbate (HCOO or CO) molecules, and $E_{H_2}(g)$ is the energy of a hydrogen molecule in the gas phase. The hydrogen adsorption energy is unchanged in the presence of one formate molecule compared with the clean surface. When two formate species occupy all In top sites at the edge, hydrogen must adsorb in an In−In bridge site, which is unfavorable. For higher formate coverage, the differential adsorption energy of hydrogen increases, due to the change in formate adsorption configuration (formate is adsorbed perpendicular to the edge). When one or more formate species are perpendicular to the edge, the hydrogen can adsorb on the Pd atom close to the row of In atoms. This adsorption site is not available when two formate species are adsorbed parallel to the edge.

On the Pd edge, the presence of CO has a destabilizing effect on hydrogen, and the differential adsorption energy of hydrogen decreases linearly with CO coverage. With a CO coverage above 0.50 ML, the adsorption energy of hydrogen becomes similar to that of the clean In edge. At a CO coverage of 1.0 ML the hydrogen atom is incorporated into the Pd edge. The computed coverage effects suggest that our calculated TOF for the methanol synthesis from CO at the Pd edge could be an overestimation as compared to the case when the effect of CO coverage is included. On the In edge, the effect of formate on the hydrogen adsorption is related to site blocking rather than repulsive interactions.

Hydrogen Reservoir Sites. Hydrogen reservoir sites, which exclusively dissociate and bind hydrogen, are often included in microkinetic models for methanol synthesis on alloy surfaces.[18,21,23,41] To compare with such models, we have considered the use of hydrogen reservoir sites. There are, in principle, two ways a reservoir site could be included: (I) Hydrogen dissociates at the reservoir site and diffuses to the other active sites where it reacts further. (II) Dissociated hydrogen reacts directly from the reservoir site with other intermediates without a diffusion step. The effect of the two types of reservoir site was investigated for the PdIn system (see SI for details and TOF plots). For both approaches, hydrogen dissociation and adsorption was defined as taking place on a separate reservoir site using the barrier and reaction energy calculated for the Pd site. For type I, the diffusion reactions from the reservoir site to the In and Pd sites were given a low barrier of 0.1 eV, and the reaction energy in each case was the difference in relative stability of the hydrogen atom at the reservoir site and the active site. This type of reservoir site does not have any appreciable effect on the overall behavior of the PdIn system. On the Pd site, the overall reaction is limited by the high CO coverage, which prevents diffusion from the reservoir site to the Pd site. On the In edge, the diffusion from the reservoir site to the In site is prevented by the relative instability of hydrogen at the In site.

In previous models, the reservoir site has been included with hydrogen reacting with other species directly from the reservoir site (type II).[18,21,23,41] We find that removing the requirement for diffusion from the reservoir site to the active sites leads to an enchanced methanol production TOF for the PdIn system. However, the physical interpretation of such a reservoir site remains unclear. Our calculations on the coverage dependence of hydrogen with respect to formate and CO shows that there are no sites available exclusively for hydrogen dissociation at or near the Pd and In edges. This indicates that to obtain a further enhancement in activity requires some other type of site to be present near the alloy edge sites. One possibility for a hydrogen reservoir site could be In_2O_3 islands on the PdIn, the presence of which have been correlated to the enhanced performance of PdIn alloy catalysts in experiments.[9,11]

5. CONCLUSIONS

We have presented DFT-based microkinetic models for the methanol synthesis reaction over PdIn, CuZn, and In_2O_3. These systems represent possible active sites for the PdIn intermetallic compound, the commercial Cu-based catalyst, and the unpromoted In_2O_3 catalyst, although the experimental catalysts include other potential active sites such as interface

https://doi.org/10.1021/acs.jpcc.2c05715
J. Phys. Chem. C 2022, 126, 15235−15246

sites. The systems were modeled with PdIn(310), Cu(211)/CuZn(211), and In_2O_3(110) surface slabs. On the PdIn(310) surface, the methanol synthesis from CO_2/CO takes place on the In and Pd edge, respectively. At low temperatures, a high selectivity toward methanol production is achieved owing to the hindering effect of CO on the RWGS reaction at the Pd site. The onset of RWGS is observed only on the Pd site at very high temperatures. Both Cu and Zn sites of the CuZn(211) surface can catalyze the MeOH synthesis, and both sites preferentially bind formate, which inhibits the reaction at low temperature. The onset of the methanol production occurs when the coverage of formate is lowered, with the methanol being produced via both the CO_2 and CO hydrogenation pathways. RWGS over CuZn(211) occurs only at very high temperatures. In contrast to the two alloy systems, In_2O_3 is active toward both methanol synthesis and the RWGS reaction at the investigated temperatures. The onset of methanol production as well as the switch-over in selectivity toward CO occur at lower temperatures on In_2O_3(110) than on PdIn(310) or CuZn(211). The mechanism for methanol synthesis follows the formate pathway on In_2O_3(110), and the In and Zn sites of the PdIn and CuZn systems. In the typical methanol synthesis temperature range of 200−300 °C, the PdIn system clearly outperforms In_2O_3 in terms of the activity and selectivity toward methanol production. Therefore, the presence of PdIn intermetallic sites could enhance the performance of Pd promoted In_2O_3 catalysts. The results also suggest that enhancing the stability of hydrogen on the surface would increase the methanol synthesis activity.

■ ASSOCIATED CONTENT

Supporting Information

The Supporting Information is available free of charge at https://pubs.acs.org/doi/10.1021/acs.jpcc.2c05715.

Details on gas-phase corrections, Arrhenius plots, and comparison of simplified rate expressions to full models and hydrogen reservoir site models (PDF)

■ AUTHOR INFORMATION

Corresponding Authors

Minttu Kauppinen − *Department of Physics and Competence Centre for Catalysis, Chalmers University of Technology, SE-412 96 Göteborg, Sweden;* orcid.org/0000-0001-8721-3719; Email: minttum@chalmers.se

Henrik Grönbeck − *Department of Physics and Competence Centre for Catalysis, Chalmers University of Technology, SE-412 96 Göteborg, Sweden;* orcid.org/0000-0002-8709-2889; Email: ghj@chalmers.se

Author

Alvaro Posada-Borbón − *Department of Physics and Competence Centre for Catalysis, Chalmers University of Technology, SE-412 96 Göteborg, Sweden;* orcid.org/0000-0002-5245-099X

Complete contact information is available at: https://pubs.acs.org/10.1021/acs.jpcc.2c05715

Notes

The authors declare no competing financial interest.

■ ACKNOWLEDGMENTS

This work was funded by the Knut and Alice Wallenberg Foundation (No: KAW 2015.0058) and the Swedish Research Council (2020-05191). The calculations were performed at C3SE via a SNIC Grant. The Competence Centre for Catalysis (KCK) is hosted by Chalmers University of Technology and financially supported by the Swedish Energy Agency and the member companies ECAPS, Johnson Matthey, Perstorp, Powercell, Preem, Scania CV, Umicore, and Volvo Group.

■ REFERENCES

(1) Jiang, X.; Nie, X.; Guo, X.; Song, C.; Chen, J. G. Recent Advances in Carbon Dioxide Hydrogenation to Methanol via Heterogeneous Catalysis. *Chem. Rev.* **2020**, *120*, 7984−8034.

(2) De, S.; Dokania, A.; Ramirez, A.; Gascon, J. Advances in the Design of Heterogeneous Catalysts and Thermocatalytic Processes for CO2 Utilization. *ACS Catal.* **2020**, *10*, 14147−14185.

(3) Zhang, X.; Zhang, G.; Song, C.; Guo, X. Catalytic Conversion of Carbon Dioxide to Methanol: Current Status and Future Perspective. *Front. Energy Res.* **2021**, *8*, 621119.

(4) Zhong, Z.; Etim, U.; Song, Y. Improving the Cu/ZnO-Based Catalysts for Carbon Dioxide Hydrogenation to Methanol, and the Use of Methanol As a Renewable Energy Storage Media. *Front. Energy Res.* **2020**, *8*, 239.

(5) Sun, J. T.; Metcalfe, I. S.; Sahibzada, M. Deactivation of Cu/ZnO/Al2O3Methanol Synthesis Catalyst by Sintering. *Ind. Eng. Chem. Res.* **1999**, *38*, 3868−3872.

(6) Kunkes, E. L.; Studt, F.; Abild-Pedersen, F.; Schlögl, R.; Behrens, M. Hydrogenation of CO2 to methanol and CO on Cu/ZnO/Al2O3: Is there a common intermediate or not? *J. Catal.* **2015**, *328*, 43−48.

(7) Martin, O.; Martín, A. J.; Mondelli, C.; Mitchell, S.; Segawa, T. F.; Hauert, R.; Drouilly, C.; Curulla-Ferré, D.; Pérez-Ramírez, J. Indium Oxide as a Superior Catalyst for Methanol Synthesis by CO2 Hydrogenation. *Angew. Chem., Int. Ed.* **2016**, *55*, 6261−6265.

(8) Wang, J.; Zhang, G.; Zhu, J.; Zhang, X.; Ding, F.; Zhang, A.; Guo, X.; Song, C. CO2 Hydrogenation to Methanol over In2O3-Based Catalysts: From Mechanism to Catalyst Development. *ACS Catal.* **2021**, *11*, 1406−1423.

(9) Snider, J. L.; Streibel, V.; Hubert, M. A.; Choksi, T. S.; Valle, E.; Upham, D. C.; Schumann, J.; Duyar, M. S.; Gallo, A.; Abild-Pedersen, F.; et al. Revealing the Synergy between Oxide and Alloy Phases on the Performance of Bimetallic In−Pd Catalysts for CO2 Hydrogenation to Methanol. *ACS Catal.* **2019**, *9*, 3399−3412.

(10) Frei, M. S.; Mondelli, C.; García-Muelas, R.; Kley, K. S.; Puértolas, B.; López, N.; Safonova, O. V.; Stewart, J. A.; Ferré, D. C.; Pérez-Ramírez, J. Atomic-scale engineering of indium oxide promotion by palladium for methanol production via CO2 hydrogenation. *Nat. Commun.* **2019**, *10*, 337.

(11) García-Trenco, A.; Regoutz, A.; White, E. R.; Payne, D. J.; Shaffer, M. S.; Williams, C. K. PdIn intermetallic nanoparticles for the Hydrogenation of CO2 to Methanol. *Appl. Catal., B* **2018**, *220*, 9−18.

(12) Rui, N.; Wang, Z.; Sun, K.; Ye, J.; Ge, Q.; Liu, C.-j. CO2 hydrogenation to methanol over Pd/In2O3: effects of Pd and oxygen vacancy. *Appl. Catal., B* **2017**, *218*, 488−497.

(13) Araújo, T. P.; Morales-Vidal, J.; Zou, T.; García-Muelas, R.; Willi, P. O.; Engel, K. M.; Safonova, O. V.; Akl, D. F.; Krumeich, F.; Grass, R. N.; et al. Flame Spray Pyrolysis as a Synthesis Platform to Assess Metal Promotion in In_2O_3-Catalyzed CO_2 Hydrogenation. *Adv. Energy Mater.* **2022**, *12*, 2103707.

(14) Lorenz, H.; Turner, S.; Lebedev, O. I.; Van Tendeloo, G.; Klötzer, B.; Rameshan, C.; Pfaller, K.; Penner, S. Pd-In2O3 interaction due to reduction in hydrogen: Consequences for methanol steam reforming. *Appl. Catal., A* **2010**, *374*, 180−188.

(15) Iwasa, N.; Mayanagi, T.; Ogawa, N.; Sakata, K.; Takezawa, N. New catalytic functions of Pd-Zn, Pd-Ga, Pd-In, Pt-Zn, Pt-Ga and Pt-in alloys in the conversions of methanol. *Catal. Lett.* **1998**, *54*, 119−123.

(16) Penner, S.; Armbruster, M. Formation of Intermetallic Compounds by Reactive Metal-Support Interaction: A Frequently Encountered Phenomenon in Catalysis. *ChemCatChem.* **2015**, *7*, 374−392.
(17) Wu, P.; Yang, B. Intermetallic PdIn catalyst for CO2 hydrogenation to methanol: mechanistic studies with a combined DFT and microkinetic modeling method. *Catal. Sci. Technol.* **2019**, *9*, 6102−6113.
(18) Wu, P.; Zaffran, J.; Yang, B. Role of Surface Species Interactions in Identifying the Reaction Mechanism of Methanol Synthesis from CO2 Hydrogenation over Intermetallic PdIn(310) Steps. *J.Phys. Chem. C* **2019**, *123*, 13615−13623.
(19) Posada-Borbón, A.; Grönbeck, H. A First-Principles-Based Microkinetic Study of CO2 Reduction to CH3OH over In2O3(110). *ACS Catal.* **2021**, *11*, 9996−10006.
(20) Studt, F.; Abild-Pedersen, F.; Varley, J. B.; Nørskov, J. K. CO and CO2 Hydrogenation to Methanol Calculated Using the BEEF-vdW Functional. *Catal. Lett.* **2013**, *143*, 71−73.
(21) Studt, F.; Behrens, M.; Kunkes, E. L.; Thomas, N.; Zander, S.; Tarasov, A.; Schumann, J.; Frei, E.; Varley, J. B.; Abild-Pedersen, F.; et al. The Mechanism of CO and CO2 Hydrogenation to Methanol over Cu-Based Catalysts. *ChemCatChem.* **2015**, *7*, 1105−1111.
(22) Behrens, M.; Studt, F.; Kasatkin, I.; Kühl, S.; Hävecker, M.; Abild-Pedersen, F.; Zander, S.; Girgsdies, F.; Kurr, P.; Kniep, B.-L.; et al. The Active Site of Methanol Synthesis over Cu/ZnO/Al2O3 Industrial Catalysts. *Science* **2012**, *336*, 893−897.
(23) Lacerda de Oliveira Campos, B.; Herrera Delgado, K.; Wild, S.; Studt, F.; Pitter, S.; Sauer, J. Surface reaction kinetics of the methanol synthesis and the water gas shift reaction on Cu/ZnO/Al2O3. *React. Chem. Eng.* **2021**, *6*, 868−887.
(24) Tameh, M. S.; Dearden, A. K.; Huang, C. Accuracy of Density Functional Theory for Predicting Kinetics of Methanol Synthesis from CO and CO2 Hydrogenation on Copper. *J. Phys. Chem. C* **2018**, *122*, 17942−17953.
(25) Niu, J.; Liu, H.; Jin, Y.; Fan, B.; Qi, W.; Ran, J. Comprehensive review of Cu-based CO2 hydrogenation to CH3OH: Insights from experimental work and theoretical analysis. *Int. J. Hydrogen Energy* **2022**, *47*, 9183−9200.
(26) Kattel, S.; Ramirez, P. J.; Chen, J. G.; Rodriguez, J. A.; Liu, P. Active sites for CO2 hydrogenation to methanol on Cu/ZnO catalysts. *Science* **2017**, *355*, 1296−1299.
(27) Chou, C.-Y.; Lobo, R. F. Direct conversion of CO_2 into methanol over promoted indium oxide-based catalysts. *Appl. Catal., A* **2019**, *583*, 117144.
(28) Kresse, G.; Hafner, J. Ab initio molecular dynamics for liquid metals. *Phys. Rev. B* **1993**, *47*, 558−561.
(29) Kresse, G.; Hafner, J. Ab initio molecular-dynamics simulation of the liquid-metalamorphous- semiconductor transition in germanium. *Phys. Rev. B* **1994**, *49*, 14251−14269.
(30) Kresse, G.; Furthmüller, J. Efficiency of ab-initio total energy calculations for metals and semiconductors using a plane-wave basis set. *Comput. Mater. Sci.* **1996**, *6*, 15−50.
(31) Kresse, G.; Furthmüller, J. Efficient iterative schemes for ab initio total-energy calculations using a plane-wave basis set. *Phys. Rev. B* **1996**, *54*, 11169.
(32) Fort, D.; Harris, I. The physical properties of some palladium alloy hydrogen diffusion membrane material. *J. Less-Common Met.* **1975**, *41*, 313−327.
(33) Dewaele, A.; Loubeyre, P.; Mezouar, M. Equations of state of six metals above 94 GPa. *Phys. Rev. B* **2004**, *70*, 094112.
(34) Henkelman, G.; Uberuaga, B. P.; Jónsson, H. A climbing image nudged elastic band method for finding saddle points and minimum energy paths. *J. Chem. Phys.* **2000**, *113*, 9901−9904.
(35) Posada-Borbon, A.; Bosio, N.; Grönbeck, H. On the signatures of oxygen vacancies in O1s core level shifts. *Surf. Sci.* **2021**, *705*, 121761.
(36) Bosio, N.; Schaefer, A.; Grönbeck, H. Can oxygen vacancies in ceria surfaces be measured by O1s photoemission spectroscopy? *J. Phys.: Condens. Matter* **2022**, *34*, 174004.
(37) Virtanen, P.; Gommers, R.; Oliphant, T. E.; Haberland, M.; Reddy, T.; Cournapeau, D.; Burovski, E.; Peterson, P.; Weckesser, W.; Bright, J.; et al. SciPy 1.0: Fundamental Algorithms for Scientific Computing in Python. *Nat. Methods* **2020**, *17*, 261−272.
(38) Campbell, C. T. The Degree of Rate Control: A Powerful Tool for Catalysis Research. *ACS Catal.* **2017**, *7*, 2770−2779.
(39) Thomas, C. A. NIST-JANAF Thermochemical Tables - SRD 132013; https://janaf.nist.gov/ (accessed November 12, 2020).
(40) Kozuch, S.; Shaik, S. How to Conceptualize Catalytic Cycles? The Energetic Span Model. *Acc. Chem. Res.* **2011**, *44*, 101−110.
(41) Studt, F.; Sharafutdinov, I.; Abild-Pedersen, F.; Elkjær, C.; Hummelshøj, J.; Dahl, S.; Chorkendorff, I.; Nørskov, J. Discovery of a Ni-Ga catalyst for carbon dioxide reduction to methanol. *Nat. Chem.* **2014**, *6*, 320−324.
(42) Cao, A.; Wang, Z.; Li, H.; Elnabawy, A. O.; Nørskov, J. K. New insights on CO and CO2 hydrogenation for methanol synthesis: The key role of adsorbate-adsorbate interactions on Cu and the highly active MgO-Cu interface. *J. Catal.* **2021**, *400*, 325−331.

https://doi.org/10.1021/acs.jpcc.2c05715
J. Phys. Chem. C 2022, 126, 15235−15246